

Regulation mechanism of Si vacancies in unintentional silicon-doped diamond by gas flow in MPCVD

Kai Yang(杨凯), Liangxue Gu(顾梁雪), Genyou Zhao(赵耕右), Kun Tang(汤琨), Bo Feng(冯博), Jiandong Ye(叶建东), Rong Zhang(张荣), Shunming Zhu(朱顺明), and Shulin Gu(顾书林)

Citation: Chin. Phys. B, 2025, 34 (**11**): 118102. DOI: 10.1088/1674-1056/ae07aa
http://cpb.iphy.ac.cn; http://iopscience.iop.org/cpb

What follows is a list of articles you may be interested in

Synthesis of two-dimensional diamond by phase transition from graphene at atmospheric pressure

Songyang Li(李松洋), Zhiguang Zhu(朱志光), Youzhi Zhang(张有志), Chengke Chen(陈成克), and Xiaojun Hu(胡晓君)

Chin. Phys. B, 2025, 34 (**5**): 058101. DOI: 10.1088/1674-1056/adb688

Pressure generation under deformation in a large-volume press

Saisai Wang(王赛赛), Xinyu Zhao(赵鑫宇), Kuo Hu(胡阔), Bingtao Feng(丰丙涛), Xuyuan Hou(侯旭远), Yiming Zhang(张羿鸣), Shucheng Liu(刘书成), Yuchen Shang(尚宇琛), Zhaodong Liu(刘兆东), Mingguang Yao(姚明光), and Bingbing Liu(刘冰冰)

Chin. Phys. B, 2024, 33 (**9**): 098104. DOI: 10.1088/1674-1056/ad58c6

Diamond-based electron emission: Structure, properties and mechanisms

Liang-Xue Gu(顾梁雪), Kai Yang(杨凯), Yan Teng(滕妍), Wei-Kang Zhao(赵伟康), Geng-You Zhao(赵耕右), Kang-Kang Fan(凡康康), Bo Feng(冯博), Rong Zhang(张荣), You-Dou Zheng(郑有炓), Jian-Dong Ye(叶建东), Shun-Ming Zhu(朱顺明), Kun Tang(汤琨), and Shu-Lin Gu(顾书林)

Chin. Phys. B, 2024, 33 (**9**): 098102. DOI: 10.1088/1674-1056/ad5aec

Synthesis and nitrogen content regulation of diamond in a high-pressure hydrogen-rich environment

Guofeng Huang(黄国锋), Liangchao Chen(陈良超), and Chao Fang(房超)

Chin. Phys. B, 2024, 33 (**6**): 068102. DOI: 10.1088/1674-1056/ad2a6d

High performance trench diamond junction barrier Schottky diode with a sidewall-enhanced structure

Ying Zhu(朱盈), Wang Lin(林旺), Dong-Shuai Li(李东帅), Liu-An Li(李柳暗), Xian-Yi Lv(吕宪义), Qi-Liang Wang(王启亮), and Guang-Tian Zou(邹广田)

Chin. Phys. B, 2023, 32 (**8**): 088101. DOI: 10.1088/1674-1056/acc2ae

---

Regulation mechanism of Si vacancies in unintentional silicon-doped diamond by gas flow in MPCVD

Kai Yang(杨凯), Liangxue Gu(顾梁雪), Gengyou Zhao(赵耕右), Kun Tang(汤琨)†, Bo Feng(冯博), Jiandong Ye(叶建东), Rong Zhang(张荣), Shunming Zhu(朱顺明), and Shulin Gu(顾书林)‡

School of Electronic Science and Engineering, Nanjing University, Nanjing 210046, *China*

(Received 2 April 2025; revised manuscript received 14 June 2025; accepted manuscript online 17 September 2025)

Diamond with silicon vacancies has an important role as a promising single-photon source applicable in the quantum information field. However, in a microwave plasma chemical vapor deposition (MPCVD) system, due to the presence of unintentional silicon doping sources such as quartz windows, the behavior of silicon vacancy formation in silicon-doped diamond is complex. In this work, the underlying mechanism of formation of silicon vacancies by unintentional silicon doping in diamond is investigated from the perspective of growing surface kinetics in a two-gas-flow MPCVD system. This system is equipped with a novel susceptor geometry designed to deliver an additional gas flow directly onto the substrate surface. Increasing the concentration of growth doping substances on the substrate surface thereby enhances the efficiency of silicon vacancy formation in diamond. At the same time, by changing the substrate deposition angle the distribution of gas and plasma on the substrate surface is changed, thereby regulating the concentration and distribution of silicon vacancies formed by unintentional silicon doping. Experimental and computational results demonstrate that the difference in silicon vacancies formed by unintentional silicon doping in diamond depends on the substances present on the substrate surface and the distribution of plasma.

Keywords: diamond, silicon vacancy, doping mechanism, unintentional doping

PACS: 81.15.Gh, 81.05.ug, 07.30.Bx, 07.30.Kf

DOI: 10.1088/1674-1056/ae07aa **CSTR:** 32038.14.CPB.ae07aa

1. Introduction

There are currently known to be more than one hundred types of vacancy defects in diamond.[1] The silicon vacancy (SiV) in diamond, a color center structure formed by a silicon atom combined with two vacancies, has garnered significant attention in recent years as an ideal single-photon source for quantum sensing and quantum communication applications.[2–5] This is attributed to the fact that 70% of its energy is concentrated at the zero-phonon line of 738 nm,[6,7] and it exhibits characteristics such as a narrow spectral width, high photon polarization and a short excitation lifetime.[8,9] In comparison, the nitrogen vacancy (NV) center has a zero-phonon line luminescence spectrum that is approximately 100 nm wide, whereas the SiV center exhibits a much narrower zero-phonon line spectrum of about 5 nm. As a result, the SiV center is better suited for applications in the field of sensing and measurement.[10,11]

Diamond materials containing SiVs can be prepared by ion implantation or chemical vapor deposition (CVD).[7,12–14] The latter is considered more promising due to its non-destructive nature and depth-selective capability.[15] In the process of depositing diamond using a microwave plasma CVD (MPCVD) system, SiVs can be formed by adding a solid silicon source or a gaseous silicon source such as silane.[16,17] However, the controllability and repeatability of the properties of SiVs prepared using either silane or solid silicon sources remain challenging.[18,19] The doping behavior of silicon in MPCVD is complex, and the doping concentration of silicon is influenced by artificial silicon sources introduced in the deposition process.[20,21] Meanwhile, unintentional silicon doping is always present. For example, the introduction of silicon dioxide from the quartz windows of the system can lead to unintentional incorporation of silicon, but this issue has received less attention.[22] Moreover, the growth and doping efficiency of diamond are affected by the gas flow distribution in the deposition system. At present, most studies focus on the influence of gas flow velocity on growth and doping but overlook the effects of gas flow input mode and substrate deposition angle.[23,24] Therefore, it is of great significance to study the doping mechanism of SiVs in diamond and improve the SiV doping concentration in diamond to improve the sensitivity of the SiV color center applied to sensor measurement.

In this work, the single-gas input mode of a MPCVD system is modified. By implementing a two-gas-flow mode, the doping gas is delivered directly to the substrate surface to study the influence of the gas delivery mode on the unintentional silicon doping concentration in diamond. Simultaneously, by changing the substrate angle, the influence of surface

†Corresponding author. E-mail: ktang@nju.edu.cn

‡Corresponding author. E-mail: slgu@nju.edu.cn

© 2025 Chinese Physical Society and IOP Publishing Ltd. All rights, including for text and data mining, AI training, and similar technologies, are reserved.

plasma distribution on the unintentional silicon doping concentration is investigated. Furthermore, to study the doping mechanism, we employ FLUENT and COMSOL numerical simulation software to analyze the gas flow distribution within the chamber under different gas delivery modes and the plasma distribution on the surface of the diamond substrate placed at different angles.

2. Experimental details

Diamond epitaxial films with SiVs were grown on (100)-oriented Ib type CVD diamond single-crystal substrates with dimensions of 3 mm×3 mm×1 mm. The substrate was double-side polished and then treated with a mixed solution of sulfuric acid and nitric acid in a 1:1 ratio at 290 °C. Subsequently, it was rinsed with acetone, ethanol and deionized water, and finally dried using nitrogen gas before deposition. Figures S1 and S2 present the photoluminescence (PL) spectra and x-ray diffraction (XRD) characterization results for the substrate surface and side surface, respectively. The PL results indicate the presence of NVs in the diamond single-crystal substrates used in this study, although their concentration is relatively low as evidenced by the PL signal intensity being significantly weaker than that of the diamond Raman peak. The XRD results reveal that both the front and side surfaces of the sample exhibit XRD peaks at 119.6°, suggesting that the crystal orientation of both surfaces is (100).[25]

A schematic diagram of the MPCVD system adopted in this experiment is shown in Fig. 1(a), with gas inlets located at both the top and bottom of the chamber. To explore the influence of gas flow mode on unintentional silicon doping, two configurations of gas input modes were employed, as shown in Fig. 1(b): in configuration (I) all gases flow from an annular pipe with holes at the top of the chamber (single-gas-flow mode) and in configuration (II) the growth gas flows from the pipe at the top of the chamber, while the doping gas flows from the pipe in the central part of the sample holder (two-gas-flow mode). Based on this two-gas-flow mode, we further investigated the impact of the placement angle of the diamond single-crystal substrate on the doping efficiency. The substrate was deposited at angles of 0°, 30°, 45° and 90° at the same position on the molybdenum substrate, as shown in Fig. 1(c).

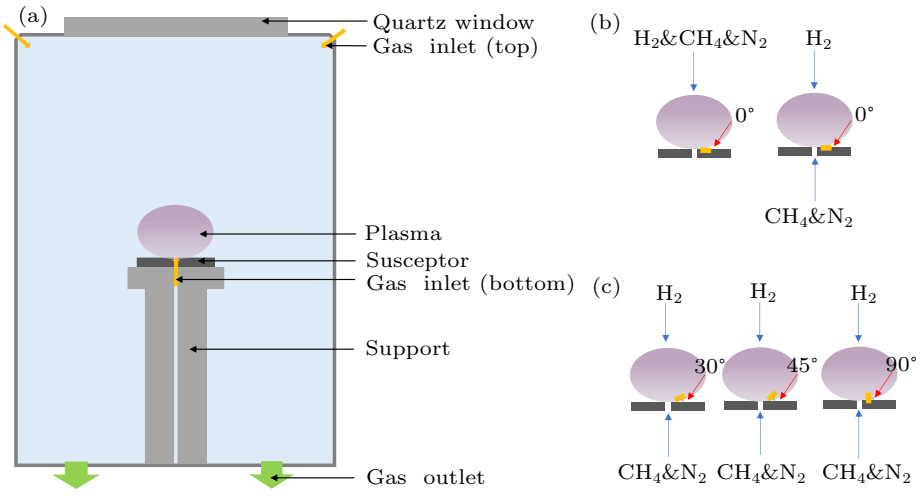


Fig. 1. (a) Schematic diagram of MPCVD chamber. (b) Two paths for the gas entering the chamber. (c) Schematic diagram of samples placed at different angles of the substrate under the two-gas-flow mode.

Research indicates that substituted nitrogen atoms in diamond increase the adsorption and desorption rates of hydrogen atoms on the diamond surface and promote the formation of SiVs.[26,27] Therefore, in this work, nitrogen is added during the experiments to investigate the influence of gas flow modes on unintentional silicon doping. Both the single-gas mode and the two-gas mode adopted the same growth conditions. The types of growth gases, flow rates, pressure and temperature in the chamber were all kept the same. The growth gases were H_2, CH_4 and N_2, with flow rates of 500 sccm, 10 sccm and 2 sccm, respectively. The pressure in the chamber was 13000 Pa, the microwave power was 3200 W, the growth temperature was 950 °C and the deposition time was 1 h. The growth temperature was monitored using an infrared laser thermometer with a laser spot size of 2 mm×2 mm. During the growth process, the laser spot was adjusted to be centered on the substrate to ensure consistent temperature measurements. In the single-gas-flow mode, all the gases (H_2, CH_4 and N_2) were introduced from the top of the chamber. In the two-gas-flow mode, H_2 was introduced from the top of the chamber while CH_4 and N_2 were introduced from the bottom of the molybdenum holder.

The optical properties of the samples were characterized by PL and micro-Raman scattering spectra using a Horiba JY HR-800 system at room temperature. The PL spectra and Raman spectra were excited by a 514 nm laser with a power of

10 mW. The samples were characterized by an X'Pert Pro MPD x-ray diffractometer to evaluate their crystal structure. To explore the internal mechanism of the effects of the single-gas-flow mode, the two-gas-flow mode and the substrates placed at different angles on the unintentional silicon doping efficiency in the MPCVD system, ANSYS FLUENT software and COMSOL Multiphysics® were used to conduct numerical simulation analysis of the gas flow and plasma distribution near the substrate. The plasma distribution inside the MPCVD discharge chamber was simulated using COMSOL. Since the MPCVD system used for deposition and growth in this work is cylindrical, a two-dimensional axisymmetric model was established to simplify the simulation process. The models and reaction equations used in COMSOL can be found in supporting file S3. The geometric models of the MPCVD chamber, the support rod and the susceptor for computational fluid dynamics simulation were created using the Design Modeler module in the ANSYS software. In the design of the model, a two-dimensional structure was adopted to simplify the calculation model.

3. Results and discussion

The PL spectra of the top and side surfaces of samples deposited under the single-gas-flow mode and the two-gas-flow mode are shown in Figs. 2(a) and 2(b). Schematic diagrams of the top and side surfaces of the sample can be found in Fig. S4(c) in the supporting information. The intensity of the PL spectra was normalized by the Raman peak at 551 nm.[28] The peaks at 575 nm and 637 nm are the characteristic peaks of NV^0 and NV^- in diamond, and 738 nm is the characteristic peak of SiV^-.[29,30] The NV^0 and NV^- centers are concentrated on the top surface of the sample, while the SiV^- centers are concentrated on the side surface of the sample.[26] It is worth noting that when comparing the single-gas-flow mode and the two-gas-flow mode there are significant differences in the formation of NVs and SiVs in the deposited diamond films. In the two-gas-flow mode, both the top and side surfaces of the sample exhibit a relatively high doping concentration. In the PL spectra of the top surfaces, the intensities of NV^0 and NV^- are both twice as high in the two-gas-flow mode. In contrast, in the PL spectra of the side surfaces, the intensity of SiV^- is 25 times higher in the two-gas-flow mode. The intensity of SiV^- is 124 times that of the Raman peak under the two-gas-flow mode, which is close to the result obtained by Agafonov *et al.*[31]

The Raman spectra of the epitaxially grown samples under two-gas-flow and single-gas-flow modes are shown in Fig. S5. A distinct diamond characteristic peak at 1332 cm^{-1} is exhibited by both the top and side surfaces of the samples in their Raman spectra, while a weak graphite characteristic peak at 1550 cm^{-1} is shown by the side surfaces.[32] The results indicate that the crystalline quality of the surfaces of the samples grown under both single-gas-flow and two-gas-flow modes is higher than that of the side surfaces. This is because the etching ability for non-diamond phases is weakened by the lower plasma intensity on the side surfaces, leading to the growth of graphite phases, whereas the formation of non-diamond phases is inhibited by the higher plasma intensity on the surfaces.

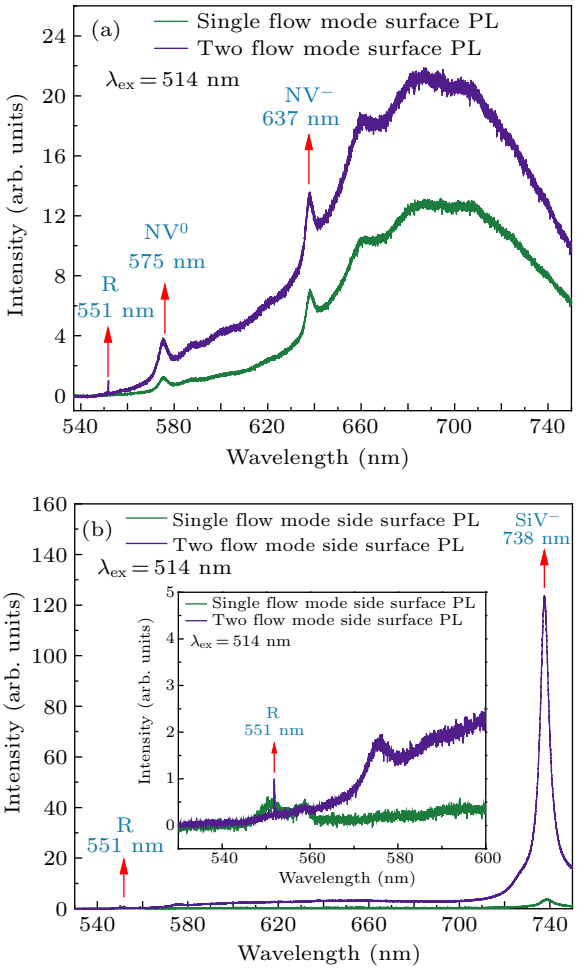


Fig. 2. (a) The PL spectra at room temperature of the deposited diamond surface under the single-gas-flow mode and the two-gas-flow mode. (b) The PL spectra at room temperature of the side surface of the deposited diamond under the single-gas-flow mode and the two-gas-flow mode.

Furthermore, we characterized the XRD patterns of the top and side surfaces of samples under single-gas-flow and two-gas-flow modes, as shown in Fig. S9. The results indicate that both the top and side surfaces of samples grown under the two modes only exhibit signal peaks at 119.6°, suggesting that the as-grown samples are single-crystal diamonds. The full width at half maximum (FWHM) of the XRD rocking curves shows that the FWHM of the top surfaces is significantly smaller than that of the side surfaces, implying that the crystalline quality of the side surfaces is poorer than that of the top surfaces. This is consistent with the results of Raman spec-

troscopy, which may be caused by trace amounts of graphite in the films.

In Fig. 2, NVs are doped on the top surface of the substrate while SiVs are mainly doped on the side surfaces of the substrate. In fact, the formation of NV and SiV centers is related to the hydrogen plasma distribution on the top surface and the sidewall of the substrate. Figures S4(a) and S4(b) in the supporting information show the hydrogen plasma profile on the top surface and side surface for the single-flow configuration by COMSOL. As can be seen, the hydrogen plasma on the top surface is around 10^{-12}, but 10^{-18} for the side surface. Therefore in Fig. 2, because the hydrogen plasma intensity determines the incorporation of NV centers, the NV concentration is much higher on the top surface than on the side and vice versa for SiVs.

Regions with high hydrogen plasma concentrations exhibit a more pronounced hydrogen etching effect, which can hinder both the growth and doping of diamond. First-principles calculations indicate that the formation energy of NVs is lower than that of SiVs.[26,33] Consequently, under identical hydrogen plasma etching conditions, NV centers are more likely to form than SiV centers. In other words, compared with SiV centers, NV centers are more prone to accumulate in regions with a high hydrogen plasma concentration while SiV centers migrate to areas with a low hydrogen plasma concentration. Compared with the single-gas-flow mode, the concentration of gases involved in doping and growth on the substrate surface is higher in the two-gas-flow mode, which results in higher doping efficiency. Therefore, the doping concentrations of SiV and NV centers are higher in the two-gas-flow mode.

This suggests that the two-gas-flow mode is more favorable for improving doping efficiency in diamond films. In the two-gas-flow mode, methane and nitrogen are introduced through small apertures beneath the susceptor to reach the substrate surface, while hydrogen is injected from the top of the chamber to generate plasma. This process confines methyl radicals and atomic nitrogen species near the susceptor, leading to an increased presence of active diamond precursor groups on the substrate surface. Additionally, atomic nitrogen enhances the dissociation of reactive gases, thereby improving the doping efficiency for SiVs and NVs within the diamond film. The growth rates of diamond films under single-gas-flow and two-gas-flow modes also confirm this view. The growth rate of the front surface of the sample was 12 $\mu m \cdot h^{-1}$ under the single-gas-flow mode while under the two-gas-flow mode it was 56 $\mu m \cdot h^{-1}$, indicating that the growth substances on the substrate surface were significantly increased under the two-gas-flow mode and thus significantly increasing the growth rate of the sample.

The formation of NV centers originates from nitrogen in the growth gas. However, during the growth process, no gas or solid substance containing silicon is intentionally added to the chamber. During the diamond deposition process using an MPCVD system, the plasma etches the quartz glass located at the top of the chamber. The silica from the quartz glass is subsequently transported into the deposition region through plasma decomposition, where it participates in the deposition growth process, leading to the formation of SiVs and resulting in unintentional silicon doping. Therefore, the silicon forming SiV^- comes from the quartz windows in the chamber. An image of the etched quartz window after disassembly of the MPCVD system is shown in Fig. S6, confirming the origin of the doped silicon.

To investigate the influence of the substrate angle on unintentional silicon doping, the substrate was placed at the same position on the molybdenum holder at 30°, 45° and 90° respectively for deposition doping under the two-gas-flow mode. When the substrate is placed at 90°, the 3 mm×1 mm surface is in contact with the Mo susceptor, and the substrate may be blown down due to disturbance of the gas flow. To prevent the substrate from being blown over, we placed it in a groove with a height of 1.2 mm, with the substrate close to the groove wall. A schematic diagram can be found in Fig. S7 in the supporting information. Figures 3(a), 3(b) and 3(c), respectively, show the distributions of the PL spectra at room temperature along the central axis of the samples grown with the substrates placed at 30°, 45° and 90°, varying with position from the bottom to the top. The axis curve length is defined in Fig. S8 in the supporting information. For the substrate placed at 90°, no diamond was deposited from the bottom up to 1200 μm. Therefore, the PL was measured starting from 1200 μm for the substrate placed at 90°. See Fig. S7 in the supporting information for a schematic of the 90° substrate.

All the PL spectral distribution diagrams varying with position are normalized by the 551 nm Raman peak. The results for the three different angles show consistent trends. From the bottom (near the molybdenum holder) to the top (far from the molybdenum holder), the spectral intensity of NVs gradually increases, while the spectral intensity of SiVs gradually decreases, exhibiting a gradient distribution with position.

Figures 3(d), 3(e) and 3(f), respectively, show distribution diagrams of the intensities of NV^0, NV^- and SiV^- along the vertical position. As shown in the figure, the intensity of NV^0 shows almost no significant change from the bottom to the top and oscillates near the horizontal line. This indicates that the angle at which the substrate is placed has a weak correlation with the formation of NV^0 in nitrogen-doped diamond. A high concentration of nitrogen atoms favors the provision of electrons to NVs, thereby forming NV^-.[34] Compared with NV^-, NV^0 is less affected by the concentration of nitrogen atoms. Our previous study showed that the plasma concentra-

tion of nitrogen atoms gradually increased from the bottom to the top of the substrate, so the gradually increasing number of nitrogen atoms provided electrons to form NV^- and had little effect on NV^0.[26] The intensity of NV^- gradually increases from the bottom to the top, while SiV^- exhibits the opposite trend, gradually decreasing from the bottom to the top. These results confirm that there is a competitive relationship between the formation of NVs and SiVs in the vertical direction during the growth of doped diamond.

From the comparison of the results for PL spectral intensity of substrates placed at three different angles, the maximum PL spectral intensity of SiV^- in the diamond film grown on the substrate placed at 45° is four times that of the substrate placed at 30° and twice that of the substrate placed at 90° (as shown by the blue curves in Figs. 3(d)–3(f)), indicating that the SiV^- content in the diamond film grown on the substrate placed at 45° is the highest. Correspondingly, the maximum intensities of NV^- for the substrates placed at 30° and 90° are equivalent, while the maximum intensity of NV^- for the substrate placed at 45° is 1.5 times that of the maximum intensities of NV^- for the substrates placed at 30° and 90° (as shown by the red curves in Figs. 3(d)–3(f)). From a comparison of the doping area results for SiVs formed by silicon doping in the PL spectra of substrates placed at three different angles, the doping area of SiV^- in the diamond film grown on the substrate placed at 45° is also the largest, at about 2250 μm×3000 μm, which is about 1.5 times that of the substrates placed at 30° and 90° (as shown by the blue curves in Figs. 3(d)–3(f)).

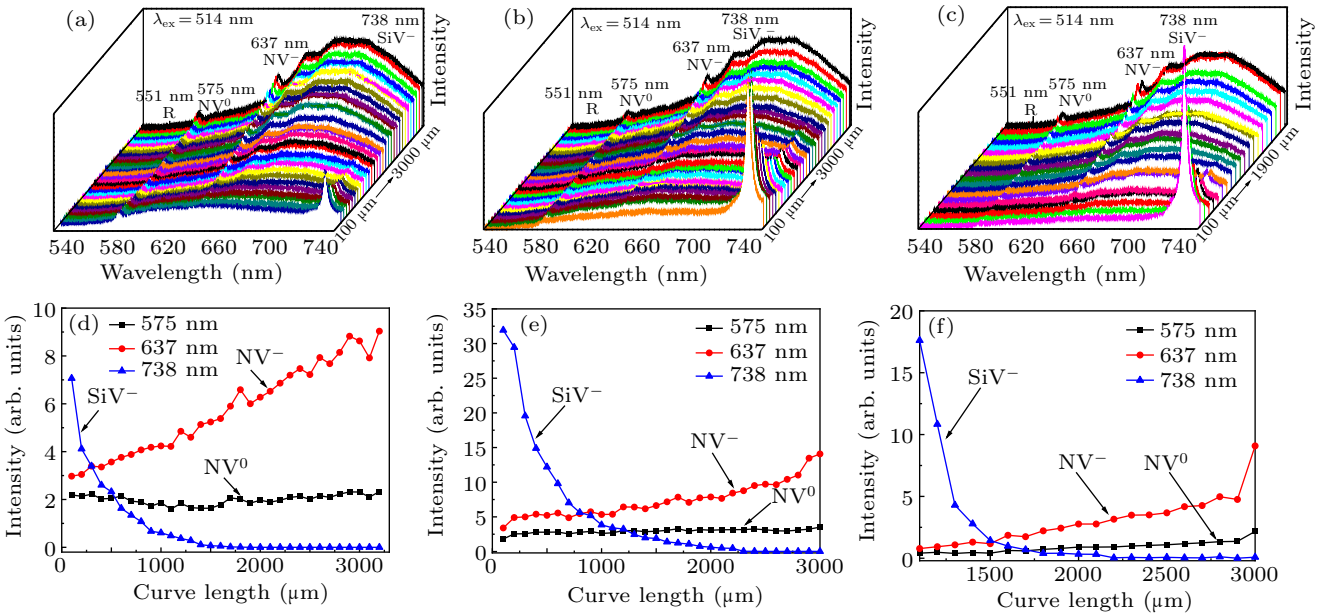


Fig. 3. The distributions of the PL spectra at room temperature along the central axis for growth samples placed at (a) 30°, (b) 45°, and (c) 90°. The distributions of PL spectral intensities of samples placed at (d) 30°, (e) 45°, and (f) 90° for NV^0, NV^- and SiV^- with position variations.

The above results indicate that the angle at which the substrate is placed has a significant impact on the formation of SiV^- in unintentionally silicon-doped diamonds growth by MPCVD. In MPCVD, the distribution of the plasma exhibits a tip effect, where the plasma tends to accumulate near the sharp edges or tips of the substrate. The placement angle of the substrate significantly influences the tip-focused accumulation of the plasma.[35] When the substrate is placed at 45°, the doping concentration and doping area of SiV^- are significantly increased. The heating of the substrate in MPCVD primarily relies on the effect of plasma. The distance between the substrate and the plasma affects the substrate surface temperature: the closer the substrate is to the plasma, the higher the surface temperature. Different placement angles of the substrate change the distance between the substrate and the plasma, thereby influencing the plasma distribution. Variations in plasma distribution lead to differences in the temperature across the substrate surface.[36] Due to the close contact between the substrate and the water-cooled holder, the effect of water cooling on the substrate is uniform, so the influence of water-cooling temperature on the plasma distribution can be ignored. When the plasma accumulates at the tip, the distribution of plasma concentration on the substrate surface differs depending on the placement angle, and the formation of SiV and NV centers is selectively influenced by the plasma temperature, resulting in the disparity in the concentration distribution of SiVs and NVs.

To investigate the mechanism between the gas flow patterns, substrate placement angle and SiV^- and NV doping efficiency, numerical simulations of the gas flow distribution in the reaction chamber under both the two-gas-flow and single-gas-flow patterns were conducted using ANSYS FLUENT

software. Figure 4(a) shows a schematic diagram of the internal model of the two-dimensional MPCVD reaction chamber. The reaction chamber consists of support rods, molybdenum substrate holders, gas inlets located at the top of the reaction chamber, gas inlets located at the bottom of the reaction chamber and gas outlets located at the bottom of the reaction chamber. Figure 4(b) shows the grid division of the two-dimensional model of the substrate support area in the MPCVD simulation reaction chamber.

Figure 5 shows the numerical simulation of the molar concentration of H_2, CH_4 and N_2 on the sample surface varying with the position of the sample surface under the single-gas-flow mode and the two-gas-flow mode. Figures 5(a), 5(b) and 5(c) present the numerical simulation of the molar concentrations of H_2, CH_4 and N_2 on a horizontally placed substrate surface as a function of position under the single-gas-flow mode. The concentration of H_2 on the substrate surface is about 0.04 kmol·m^{-3}, the concentration of CH_4 is 1×10^{-4} kmol·m^{-3} and the concentration of N_2 is 1×10^{-5} kmol·m^{-3}. Under the single-gas-flow mode, the molar concentrations of H_2, CH_4 and N_2 on the substrate surface are uniformly distributed and show no significant variation with position. Figures 5(d), 5(e) and 5(f) show the numerical simulation of the molar concentrations of H_2, CH_4 and N_2 on the horizontally placed substrate surface varying with the position of the sample surface under the two-gas-flow mode. Under the two-gas-flow mode, the distributions of H_2, CH_4 and N_2 on the substrate surface exhibit a gradient distribution.

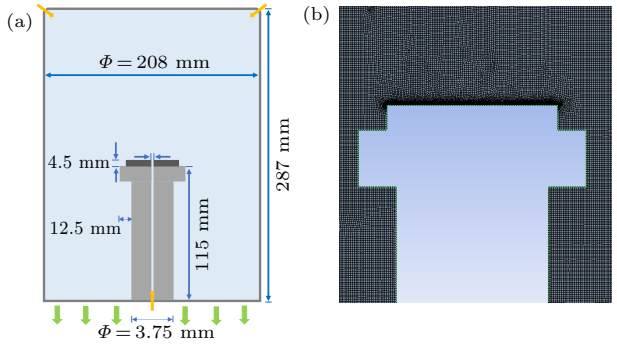


Fig. 4. (a) Schematic diagram and dimensions of the two-dimensional simulation chamber of the MPCVD. (b) Grid generation for the substrate support region in a two-dimensional model of the MPCVD simulation reactor.

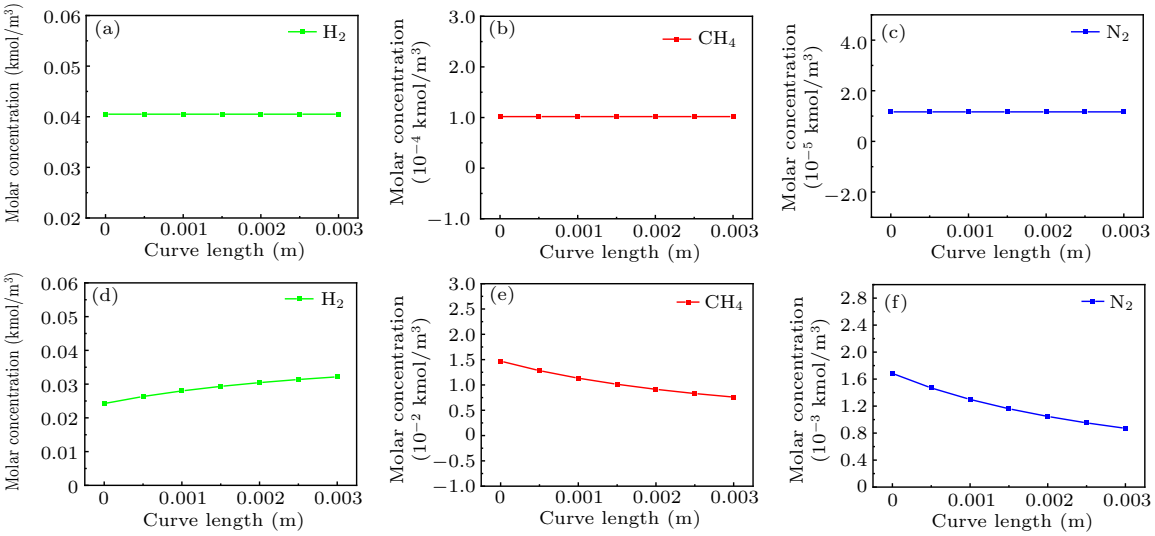


Fig. 5. The distributions of (a) H_2, (b) CH_4 and (c) N_2 molar concentrations with position on the sample surface under the single-gas-flow mode. The distributions of (d) H_2, (e) CH_4 and (f) N_2 molar concentrations with position on the sample surface under the two-gas-flow mode.

As shown in Fig. 5(d), the H_2 concentration on the side of the substrate surface close to the bottom inlet hole is lower than that on the side far from the bottom inlet hole. The hydrogen concentration at the lowest point is about 0.24 kmol·m^{-3}, and the hydrogen concentration at the highest point is about 0.32 kmol·m^{-3}. Due to the convective influence of the CH_4 and N_2 introduced from the bottom inlet hole, the concentrations of CH_4 and N_2 exhibit the opposite trend to the H_2 concentration. The maximum concentrations of CH_4 and N_2 on the substrate surface are about 0.015 kmol·m^{-3} and 0.0017 kmol·m^{-3}, respectively, and the minimum concentrations are 0.008 kmol·m^{-3} and 0.0009 kmol·m^{-3}, respectively. Compared with the single-gas-flow mode, the molar concentrations of CH_4 and N_2 on the substrate surface in the two-gas-flow mode are one order of magnitude higher, while the concentration of H_2 remains at the same order of magnitude. The computational results align with our experimental findings, indicating that in the two-gas-flow mode, methane and nitrogen are localized on the support surface. This localization enhances the concentration of active methyl radicals and nitrogen atom groups near the substrate, thereby improving doping and deposition efficiency.

The plasma electron temperatures on the substrate surface at 30°, 45° and 90°, simulated by COMSOL are shown in Figs. 6(a), 6(b) and 6(c). The simulation results indicate that the electron temperature of the plasma on the substrate sur-

face gradually increases from the bottom to the top of the substrate. For the substrate placed at 30°, the interval where the electron temperature is lower than 2.7 eV is 1500 μm. For the substrate placed at 45°, the interval where the electron temperature is lower than 2.7 eV is 2000 μm. For the substrate placed at 90°, the interval where the electron temperature is lower than 2.7 eV is also 1500 μm, which is consistent with the interval for the formation of SiV^- in Fig. 3. A high electron temperature indicates a high concentration of hydrogen plasma, and a higher concentration of hydrogen plasma results in a stronger etching effect. The varying etching strength of hydrogen plasma leads to different distributions of SiVs and NVs during doping. First-principles calculations show that the formation energy of NVs in diamond is lower than that of SiVs, which means that NVs are more likely to form under the same etching conditions. Therefore, NVs tend to accumulate in areas with high electron temperature while SiVs tend to accumulate in areas with low electron temperature. This is consistent with the experimental results shown in Fig. 3.

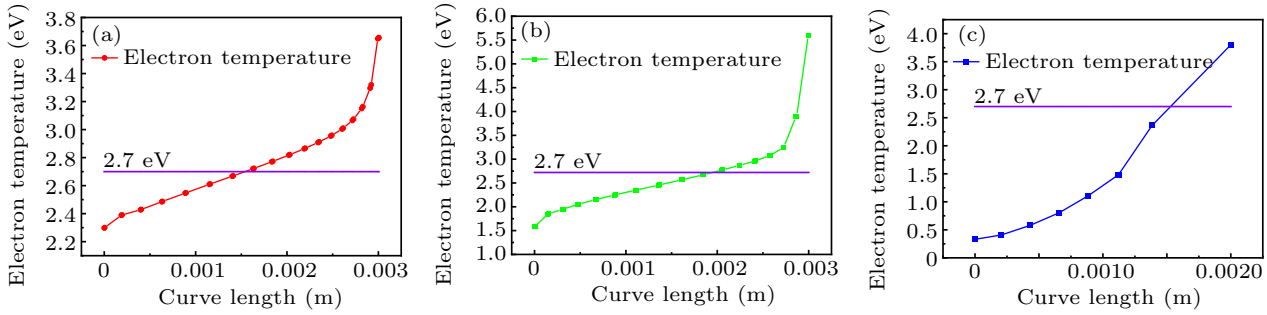


Fig. 6. The distribution of plasma electron temperature varying with the position on the substrate surface of samples placed at 30°, 45° and 90°.

4. Conclusion

In summary, we have designed a novel two-gas-flow mode in a MPCVD system which can directly deliver gases to the substrate surface and increase the dopant concentration on the substrate surface. Compared with the single-gas mode, in the two-gas-flow mode substances such as methane and nitrogen are directly transported from the small holes at the bottom of the susceptor to the substrate surface and localized on the substrate surface, thereby increasing the doping concentrations of NVs and SiVs in the sample. Furthermore, the influence of substrate angle on unintentional silicon and nitrogen doping, leading to the formation of SiVs and NVs, was studied in the two-gas-flow mode. Different substrate placement angles affect the distribution of plasma on the substrate surface. The formation of NVs and SiVs varies with the electron temperature distribution. NVs tend to form in regions on the substrate with high electron temperature, while the formation of SiVs exhibits the opposite trend. At a substrate placement of 45°, unintentional silicon doping demonstrates better doping efficiency and a large doping area compared with other substrate angles. This work provides a new approach for MPCVD systems to control unintentional silicon doping and offers a novel method for improving the doping efficiency of substances in MPCVD systems.

Acknowledgements

This work was supported by the National Natural Science Foundation of China (Grant No. 62274084) and the Fundamental Research Funds for the Central Universities (Grant No. 0210-14380193).

References

[1] Mzyk A, Ong Y, Ortiz Moreno A R, Padamati S K, Zhang Y, Reyes-San-Martin C A and Schirhagl R 2021 *Anal. Chem.* **94** 225
[2] Tzeng Y K, Ke F, Jia C, Liu Y, Park S, Han M, Frost M, Cai X, Mao W L and Ewing R C 2024 *Nat. Commun.* **15** 7251
[3] Wu Y and Weil T 2022 *Adv. Sci.* **9** 2200059
[4] Yang C, Mi Z, Jin H, Venkatesan T, Vispute R and Bettiol A A 2023 *Carbon* **203** 842
[5] Bradac C, Gao W, Forneris J, Trusheim M E and Aharonovich I 2019 *Nat. Commun.* **10** 5625
[6] Liu Y, Guo Q, Cai Z, Wang Z, Zhao H, Li B, Li M, Chen L, Ma H and Jia X 2023 *J. Cryst. Growth* **619** 127346
[7] Evans R E, Sipahigil A, Sukachev D D, Zibrov A S and Lukin M D 2016 *Phys. Rev. Appl.* **5** 044010
[8] Sukachev D D, Sipahigil A, Nguyen C T, Bhaskar M K, Evans R E, Jelezko F and Lukin M D 2017 *Phys. Rev. Lett.* **119** 223602
[9] Zhang T, Gupta M, Jing J, Wang Z, Guo X, Zhu Y, Yiu Y C, Hui T K, Wang Q and Li K H 2022 *J. Mater. Chem. C* **10** 13734
[10] Choi S, Agafonov V N, Davydov V A and Plakhotnik T 2019 *ACS Photonics* **6** 1387
[11] Choi S, Agafonov V N, Davydov V A, Kulikova L F and Plakhotnik T 2020 *Nanotechnology* **31** 205709
[12] Lagomarsino S, Flatae A, Kambalathmana H, Sledz F, Hunold L, Soltani N, Reuschel P, Sciortino S, Gelli N and Massi M 2021 *Front. Phys.* **8** 601362
[13] Titze M, Byeon H, Flores A, Henshaw J, Harris C T, Mounce A M and Bielejec E S 2022 *Nano Lett.* **22** 3212
[14] Yang B, Li H, Yu B, Lu J, Huang N, Liu L and Jiang X 2021 *Carbon* **171** 455
[15] Raj R, Pradeep K and Rao M 2024 *Bull. Mat. Sci.* **47** 1
[16] Guo X, Yang B, Zhang X, Lu J, Huang M, Huang N, Liu L and Jiang X 2024 *J. Mater. Chem. C* **12** 15483
[17] Lin W, Lv X, Wang Q, Li L and Zou G 2024 *Mater. Sci. Semicond. Process* **180** 108554
[18] Sedov V, Ralchenko V, Khomich A, Vlasov I, Vul A, Savin S, Goryachev A and Konov V 2015 *Diam. Relat. Mat.* **56** 23
[19] Bolshakov A, Ralchenko V, Sedov V, Khomich A, Vlasov I, Khomich A, Trofimov N, Krivobok V, Nikolaev S and Khmelnitskii R 2015 *Phys. Status Solidi A-Appl. Res.* **212** 2525

[20] Sedov V, Khomich A, Ralchenko V, Martyanov A, Savin S, Poklonskaya O and Trofimov N 2015 *Journal of Coating Science and Technology* **2** 38

[21] Dietrich A, Jahnke K D, Binder J M, Teraji T, Isoya J, Rogers L J and Jelezko F 2014 *New J. Phys.* **16** 113019

[22] Di Liscia E J, Reinoso M, Álvarez F and Huck H 2019 *Appl. Phys. A-Mater. Sci. Process.* **125** 1

[23] Emelyanov A, Pinaev V, Plotnikov M Y, Rebrov A, Timoshenko N and Yudin I 2022 *J. Phys. D-Appl. Phys.* **55** 205202

[24] Croot A, Mahoney E J, Dominguez-Andrade H, Ashfold M N and Fox N A 2020 *Diam. Relat. Mat.* **109** 108011

[25] Tomita S, Burian A, Dore J C, LeBolloch D, Fujii M and Hayashi S 2002 *Carbon* **40** 1469

[26] Yang K, Teng Y, Zhao W, Tang K, Fan K, Duan J, Huang Y, Ye J, Zhang R and Zhu S 2024 *Vacuum* **222** 113027

[27] Zaitsev A, Moe K and Wang W 2018 *Diam. Relat. Mat.* **88** 237

[28] Liu D, Hao L, Chen Z, Zhao W, Shen Y, Bian Y, Tang K, Ye J, Zhu S and Zhang R 2020 *Appl. Phys. Lett.* **117** 022101

[29] Aprà P, Amine N H, Britel A, Sturari S, Varzi V, Ziino M, Mino L, Olivero P and Picollo F 2024 *Adv. Funct. Mater.* **39** 2404831

[30] Khomich A A, Sektarov E S, Boldyrev K, Ralchenko V, Bolshakov A P, Khmelnitsky R A and Sedov V 2024 *Opt. Mater.* **157** 116206

[31] Plakhotnik T, Duka T, Davydov V A and Agafonov V N 2023 *Diam. Relat. Mat.* **139** 110363

[32] Thapliyal V, Alabdulkarim M E, Whelan D R, Mainali B and Maxwell J L 2022 *Diam. Relat. Mat.* **127** 109180

[33] Mansoor M, Mansoor M, Mansoor M, Aksoy A, Seyhan S N, Yıldırım B, Tahiri A, Solak N, Kazmanlı K and Er Z 2022 *Diam. Relat. Mat.* **126** 109072

[34] Collins A T 2002 *J. Phys-Condens. Matter* **14** 3743

[35] Fernandes A, Silva V, Carrapichano J, Dias G, Silva R and Costa F 2001 *Diam. Relat. Mat.* **10** 803

[36] Yang B, Shen S, Zhang L, Shen Q, Zhang R, Zhang Y, Gan Z and Liu S 2022 *J. Appl. Crystallogr.* **55** 240